Local analysis of oxygen reduction catalysis by scanning vibrating electrode technique : a new approach to the study of biocorrosion

Hicham Iken, Luc Etcheverry, Alain Bergel, Régine Basséguy

Local analysis of oxygen reduction catalysis by scanning vibrating electrode technique: a new approach to the study of biocorrosion

Hicham IKEN, Luc ETCHEVERRY, Alain BERGEL*, Régine BASSEGUY

Laboratoire de Génie Chimique CNRS, 5 rue Paulin Talabot BP 1301, 31062 Toulouse, France.

ABSTRACT

The Scanning Vibrating Electrode Technique (SVET) was employed to investigate oxygen reduction catalysis by the presence of enzyme in an aerobic medium. Heme protoporphyrin (hemin) was chosen as a model of the enzymes that are able to catalyze oxygen reduction. A strict experimental protocol was defined for preparing the graphite surface by deposition of hemin with a simple configuration mimicking the presence of enzyme on the samples. The same configuration was adapted to a stainless steel electrode. Different geometric arrangements were investigated by SVET to approach the local conditions. The results demonstrated that hemin deposited on the electrode surface led to an increase in the cathodic current, which indicated a catalytic effect. Based on the SVET analysis, it was demonstrated that hemin caused the appearance of galvanic cells on the material surface. The SVET proved able to locate active catalytic centres and therefore to foresee the contribution of the enzyme to the creation of galvanic cells, thus leading to localized corrosion. The application of SVET to the study of the interaction between biological molecules and material provides a new approach for visualizing and understanding microbially influenced corrosion (MIC) in an aerobic medium.

Keywords: SVET; oxygen reduction catalysis; hemin; graphite; stainless steel.

* Alain BERGEL; Tel. (33) 5 34 61 52 48 ; Fax. (33) 5 34 61 52 53; e-mail : Alain.Bergel@ensiacet.fr

INTRODUCTION

The biodeterioration of materials due to biofilm formation has great environmental and economic implications. Many industrial installations suffer from corrosion problems as a result of biofilm development. In the aim of preventing and controlling biocorrosion, a variety of techniques are currently employed to collect information, understand the phenomenon and the determine factors and parameters that control it.

The application of electrochemical techniques in the investigation of biocorrosion is based on the determination of electrochemical parameters in the macro range (corrosion potential, corrosion rate, anodic and cathodic currents, open circuit potential, etc.). These techniques inform on the changes in the electrochemical behaviour of the material in biofilm development conditions.

On the other hand, chemical spectroscopy of the surfaces offers qualitative and semi-quantitative information on the nature of the deterioration products that have accumulated on a metal surface [1-4]. Microscopy provides information about the morphology of the microbial cells and colonies, the distribution of microbial colonies on the surface and the nature of the corrosion products. It also reveals the type of attack by revealing changes in the metal microstructure after removal of the biofilm [5-9]. Surface chemical analysis using X-ray diffraction (XRD) and energy dispersive X-ray analysis (EDX) have also been widely used to obtain information on elementary corrosion products on metal surfaces [10].

In contrast, the Scanning Vibrating Electrode Technique (SVET) appears to be a powerful electrochemical technique for studying oxidation-reduction reactions in the micro range [11]. This technique offers the possibility of mapping microscale variations in current densities over a metal surface by measuring the potential gradients developed in the solution due to the ionic

flow, and has a wide range of applications in the study of corrosion phenomena [12–15]. The maps show the spatial distribution of anodic and cathodic zones over the surface. SVET is used in situ to measure the current densities above surfaces without altering the corrosion process or changing the local environment of the sites or the conductive and electrochemical parameters. The technique has rarely been applied to biocatalysis. An early local study applied to MIC demonstrated that having 2 % of the surface occupied by cathodic sites where oxygen reduction was catalyzed was sufficient to cause an increase of two orders of magnitude in the current with sea-water biofilms [16]. Thus, SVET is an electrochemical technique applying to local analysis and is well suited to the study of biocorrosion.

In previous works on biocorrosion, it has been observed that the free corrosion potential of stainless steel is more anodic when the material is immersed in aerated natural sea-water than when it is in a synthetic medium [17,18]. The risk and the severity of localized corrosion onset are consequently increased by the adhesion of marine biofilms [19]. The passive current is the same in the two media, proving that no modification of the anodic phenomena occurs [20]. However, aerobic biocorrosion of metal surfaces or aerobic MIC (microbially influenced corrosion) occurs because of catalysis of the oxygen reduction reaction by the biofilm [20,21].

Although the mechanisms are still a subject of controversy, several hypotheses have been proposed to explain this catalysis: the formation of hydrogen peroxide [22], modification of the oxides on the material surface [23] or the presence of biological molecules (enzymes such as peroxidase and catalase) that intervene in the various steps of oxygen reduction [24]. Several studies attribute the increase or ennoblement of the free corrosion potential (E_{corr}) of stainless steel in oxygenated natural waters to enzymes, the activities of which have been detected in biofilms [25-29]. This hypothesis is supported by the detection of superoxide dismutase and

peroxidase activities in some marine biofilms [30,31]. In our laboratory, it has been observed that catalase adsorbed on a glassy carbon surface efficiently catalyzes oxygen reduction via direct electron transfer from the electrode [24, 32]. The results have been discussed with respect to the electrode surface properties (hydrophilic/hydrophobic forces) and the enzyme structure: to be efficient, the heme group of the catalase must be as close as possible to the electrode surface.

A preliminary work showed that the immobilization of hemin on a stainless steel surface clearly shifted the corrosion potential toward anodic values and that the potential displacement of E_{corr} in current-potential curves was linked to the increase in the cathodic current of oxygen reduction [16]. Hemin is a protoporphyrin heme group without the protein shell and with FeII/FeIII as the redox active centre that allows the oxygen link. Although the catalysis effect has been shown [16], the contribution of hemin to the promotion of material corrosion has not been demonstrated.

The present investigation was undertaken to study oxygen reduction catalysis by hemin in an aerobic medium using the scanning vibrating electrode technique. The first experiment consisted of the immobilization of hemin using dimethylsulfoxide (DMSO) on a graphite surface. Then the proposed model was applied to a stainless steel surface to evaluate the influence of hemin on the electrochemical behaviour of this material. It is often advanced that the biofilm promotes galvanic coupling, thus influencing the electrochemical behaviour of metal and so generating localized corrosion [33]. To the best of our knowledge, no previous study has displayed such galvanic coupling created by catalysis (whether biological or not).

In this work, several configurations were used to simulate the action of enzymes on the material surface and the action of the biofilm to create galvanic coupling. It was proposed that, by

adjusting SVET to biocorrosion investigations, it would be possible to elucidate the role of biological molecules in the biocorrosion phenomenon.

EXPERIMENTS

Hemin and dimethylsulfoxide (DMSO) were purchased from Fluka and Aldrich respectively. The stainless steel electrodes were made of URB 66 (percentage composition by weight: 23.92 Cr, 21.90 Ni, 5.44 Mo, 2.99 Mn 1.86 W, 1.54 Cu, 0.47 N, 0.014 N, 0.001 S, bulk iron) provided by Creusot Loire Industrie (Le Creusot, France). Electrodes were 3mm x 5mm rectangles embedded in epoxy resin (Stuers, Epofix Kit), polished successively with P120, P180, P400, P800, P1200, P2400 and P4000 abrasive papers (Lam Plan) and then rinsed with distilled water. To obtain reproducible oxidation states, an 18-hour polarization at constant potential (-0.50 V/SCE) in 0.50M NaCl solution was performed before each experiment. Pyrolytic graphite electrodes, purchased from Le Carbone Lorraine (France) were 6.15 mm diameter cylinders embedded in epoxy resin. The electrodes were polished successively with P240, P400, P1200 and P2400 abrasive papers and then rinsed with distilled water. For cyclic voltammetry tests with hemin, a drop of Hemin-DMSO solution (1mg/mL) was deposited on the electrode surfaces and left for 15 minutes before each analysis. For SVET analysis, hemin was deposited only on a part of the electrode surface, the rest being masked under Teflon rubber. After this preparation, the surface has a part with adsorbed hemin and a part free of any deposit Details of the configurations used for SVET analysis are given in the description of the results.

A 4-channel potentiostat (VMP2, Princeton Applied Research) was used for cyclic voltammetry. The electrochemical setup included a saturated calomel electrode (SCE) as the reference and a platinum electrode as the auxiliary. Cyclic voltammograms were plotted in the cathodic direction

from E_{corr} to – 1.0 V/SCE at scan rates of 0.1V s^{-1} for graphite and 0.01V s^{-1} for stainless steel in NaCl solution (0.5M).

Local current measurements were performed using a SVET from Applicable Electronics (USA). Pt–Ir microelectrodes (Micro Probe Inc., USA) were black platinized before being used as probes. The diameter of the sphere of black platinum deposit was about 20µm with a corresponding capacitance of around 40 nF. The amplitude of the vibration was about 20µm and the vibration frequencies were in the 200 to 300 Hz range along the *X* and *Z* directions. The microprobe was moved using a computer controlled XYZ micromanipulator. A video camera was used to image the distance between the microprobe and the sample surface. The setup parameters (area of surface analyzed, scan type, number of steps, time, etc.) were controlled by the ASET Software (Science Wares Inc., USA), which also converted the potential drop to a current density value. The data were then processed with Matlab software and the current density was plotted as a three-dimensional surface with the current density measured along the *Z*-axis as a function of the *X*, *Y* plane. In this format, positive and negative current densities represent anodic and cathodic sites respectively. All the experiments were performed at a distance of 100µm above the surface in NaCl 1mM solution (conductivity 0.15 mS cm^{-1}) either at open circuit or under fixed potential at room temperature. For the latter configuration, as in voltammetric analysis, the saturated calomel electrode (SCE) was used as the reference electrode. A circular thread of platinum was used as the auxiliary electrode around the surface analyzed (fig. 1) in order to obtain a controlled configuration of field lines (axial symmetry).

RESULTS

Voltammetric analysis

Figure 2 gives the voltammetric curves at the scan rate 0.1V/SCE in NaCl 0.5 M obtained for a clean graphite electrode and for hemin adsorbed from DMSO on the graphite surface. Without hemin, the reduction of oxygen starts at about -0.35 V/SCE, no diffusion limitation can really be observed. When hemin is adsorbed on graphite, the oxygen reduction starts before at about + 0.1 V/ECS and the cathodic current was higher in the whole range of potentials scaned (from + 0.1 to -1.0 V/ECS). At -0.35 V/SCE the current was 2.8 times as high in the presence of hemin.

Cyclic voltammograms obtained in NaCl 0.5 M at a scan rate of 0.01 V s^{-1} for stainless steel samples are reported in figure 3. The two curves, drawn with and without hemin, show a broad cathodic peak corresponding to the reduction of oxygen. The presence of hemin significantly increased the current in the cathodic domain and at -0.50 V/SCE the current was about 1.7 times as high in the presence of hemin.

For both graphite and stainless steel electrodes, adding hemin significantly increased the cathodic current. Hemin adsorbed on the surface catalyzed the electrochemical reduction of oxygen via direct electron transfer from the electrode to hemin, as previously shown on glassy carbon [32]. Adsorption of hemin on the electrode surface could be regarded as a model for the action of biofilm in an aerobic medium. These results concern the catalytic activity of hemin towards oxygen reduction on graphite and stainless steel electrodes but no information was obtained on the corrosion process affecting these materials.

SVET analysis

SVET analysis was used to observed local currents on electrodes at a cathodic imposed potential or at the open circuit potential. The SVET microprobe scanned 100µm above the surface.

The first SVET microprobe scans were performed over control samples where the surface had been pre-treated with DMSO alone. Then certain areas of the experimental electrodes were pre-treated with DMSO containing hemin. The electrodes were maintained under the cathodic potential imposed during scanning. The imposed potential was the potential value where the highest difference of cathodic current was recorded on cyclic voltammograms with and without hemin (fig. 2 and 3): -0.35 V/SCE for graphite and -0.50 V/SCE for stainless steel.

For graphite surface-treated with DMSO alone, the SVET map showed a uniform distribution of current over the surface and the mean current densities values were negative, around -0.5µA cm^{-2} (fig. 4A).

Then, hemin dissolved in DMSO was deposited on only a part of the graphite surface, thus delimiting two distinct zones: with hemin on the left / without hemin on the right. The current map made at the same imposed potential (-0.35 V/SCE) on the interface between the two areas with and without hemin is reported in figure 4B. Two different domains were observed: on the left side of the sample (with hemin), the currents were at least 5 times more negative than on the right (without hemin), showing a strong cathodic behaviour in the left-hand zone compared to the right. The mean value of the current observed over the zone without hemin (free of any deposit) was almost the same than that observed over surface treated with DMSO alone (Fig. 4A), showing no effect of DMSO alone. In conclusion, it can be clearly seen that the presence of hemin strongly shifted the surface current to more negative values.

As for the case on graphite, mixed surfaces with and without hemin were prepared on stainless steel and scanned with a SVET microprobe. Preliminary scans were carried out on a stainless steel surface treated with DMSO alone at an imposed potential of -0.50 V/SCE (fig. 5A). The SVET map showed a uniform distribution of current densities over the surface in the cathodic domain, as for the graphite sample. Then, when hemin was deposited on one half of the stainless steel surface, two distinct areas were observed (fig. 5B). The hemin zone took more cathodic current values (-2 to -4 µA cm^{-2}) in contrast with the area without hemin, where negative currents were weaker (around -0.5µA cm^{-2}). These results show the catalysis of oxygen reduction on graphite and stainless steel surfaces where hemin has been deposited.

The next configuration chosen for graphite and stainless steel surfaces involved depositing hemin on a circular zone about 500 µm in diameter (fig. 6). The SVET map recorded for graphite during polarization at -0.35 V/SCE is illustrated in figure 7. Hemin deposited on the 500-µm-diameter circular area on the surface led to the appearance on the SVET map of a cathodic peak over this zone with a maximum current value of -1.65 µA cm^{-2}. The surrounding zone presented also cathodic current densities with a mean value of XX µA cm^{-2}. This clearly shows that hemin creates efficient cathodic zones when it is deposited on a material surface and SVET allows this catalysis to be displayed.

As for graphite, the SVET map was recorded at -0.5 V/SCE on the stainless steel surface where hemin had been deposited on a 500-µm-diameter circular area (fig. 8). On the map, a cathodic peak indicating a strong cathodic activity appeared in the hemin zone (maximum -5 µA cm^{-2}) while the current was smaller (-1µA cm^{-2}) in the surrounding zones without hemin.

The last configuration (fig. 9) was the opposite of the previous one: a clear area 500µm in diameter was protected with a Teflon pen and hemin was deposited around this zone. The SVET map showed cathodic behaviour around the non-hemin zone, within which the trend was towards the appearance of an anodic peak (0.1µA cm^{-2}). This configuration modelled a pit on the material surface that illustrated a biocorrosion phenomenon.

By comparing the SVET analyses obtained under an imposed potential and the curves obtained in the voltammetry study, it is seen that the catalytic effect of hemin is better put in light on SVET scan than on voltammograms: higher ratios of the current densities with and without hemin are found in SVET analysis. This is linked to the analysis scale: with SVET, the current density recorded comes from a very small and then homogeneous surface, whereas in voltammetry the current density is the global response of the whole surface that can present heterogeneities in the distribution of the catalyst. Hicham modifie sit u trouves que ça ne va pas bien

Other SVET analyses were performed with the various configurations (DMSO alone, interface hemin zone / without hemin zone). The SVET map showed a uniform distribution of current over the graphite surface pre-treated with DMSO alone (fig. 10A): anodic and cathodic zones were randomly distributed with current densities between 1.5 and -1.5 µA cm^{-2}.

The second scan at open circuit potential was achieved above the interface between the zones with and without hemin and is presented in figure 10B. The current map showed two distinct areas with two different behaviours. On the left, where hemin was deposited, the current distribution was uniform with current densities around -2 µA cm^{-2}. In contrast, the right hand side, without hemin, showed positive current peaks of 5 to 10µA cm^{-2} indicating a strong anodic activity in this zone. In comparison to the first map (fig. 10A), the presence of hemin on one half

of the surface caused the apparition of local anodic sites on the opposite side. A galvanic cell had been created.

The same experiments were carried out on a stainless steel electrode at open circuit potential (fig. 11). The distribution of current densities on the surface was uniform and varied between 1.5 and -2µA cm^{-2} for the electrode modified by DMSO only. When hemin was deposited on one half of the surface, two electrochemically distinct zones appeared. In the hemin side, the current densities were slightly negative (around -1µA cm^{-2}) but, on the opposite side, anodic peaks appeared with current values that exceeded 10µA cm^{-2}.

Thus, hemin deposited on graphite or stainless steel creates a galvanic coupling in the material surface, involving strong anodic activity in the areas without hemin and localized corrosion can thus be expected.

Both techniques (cyclic voltammetry and SVET) helped to demonstrate the ability of hemin to catalyze oxygen reduction in an aerobic medium. Nonetheless, SVET revealed that hemin adsorbed on the material surface leads to the apparition of galvanic cells: corrosion can be found where hemin has not been deposited. SVET proved to be a very powerful tool for determining the interactions of a biological molecule with graphite and stainless steel surfaces, revealing information which would not have been obtained using other approaches.

CONCLUSION

The catalysis of oxygen reduction on graphite and stainless steel electrodes by hemin was investigated using the cyclic voltammtry and the Scanning Vibrating Electrode Technique in an

aerobic medium. A strict experimental protocol was defined to prepare sample surfaces by deposition of hemin dissolved in DMSO.

CVs showed an increase in cathodic current when hemin was immobilized on the sample surfaces, indicating catalysis of oxygen reduction. This simple configuration for mimicking the presence of enzyme (perhaps a biofilm) on the samples was adopted for SVET analysis and different geometric arrangements were investigated by SVET to approach the local conditions. When a cathodic potential was imposed, the presence of hemin was made visible by the value of the cathodic current on the SVET maps: the no-hemin zone was distinguished from the hemin-modified zone by a current at least 4 times more negative, in agreement with a catalytic effect. At open circuit potential, positive current peaks appeared on the clean zones in contrast with the hemin adsorbed ones. This can be ascribed to be the beginning of localized corrosion.

This is the first time that a galvanic cell has been clearly observed as a result of the presence of a biological molecule on a material surface. This original result of our work concerns aerobic biocorrosion as a consequence of microbial catalysis of oxygen reduction. By accessing the centres where biocatalysis takes place, SVET has been shown to be a powerful technique for investigating microbially influenced corrosion.

ACKNOWLEDGMENTS

We would like to thank Maria Elena Lai who had the innovative idea of immobilizing enzyme using adsorption from DMSO, Rolf Gubner from Kimab (Stockholm) for his kind help with the SVET implementation, the network ERG+ “surface of materials in living environments (SMILE)” and l’Agence Universitaire de la Francophonie (AUF) for their financial support.

REFERENCES

[1] G. G. Geesey, R. J. Gillis, R. Avci, D. Daly, M. Hamilton, P. Shope, G. Harkin, Corrosion Science 38 (1996) 73.

[2] J. Pendyala, R. Avci, G.G. Geesey,P. Stoodley, M. Hamilton, G. Harkin, Journal of Vacuum Science and Technology 14 (1996) 1755.

[3] P. Suci, K. J. Siedlecki,R. J. Palmer,D. C. White,G. G. Geesey, Applied and Environmental Microbiology 63 (1997) 4600.

[4] I. B. Beech, R. Gubner,V. Zinkevich, L. Hanjangsit, R. Avci, Corrosion 99, NACE, Houston, TX, USA (1999) 185.

[5] B.J. Little, P.A Wagner, R.I. Ray, R. Pope, R. Sheetz, Journal of Industrial Microbiology 8 (1991) 213.

[6] P.A. Wagner, R. I. Ray, American Society for Testing and Materials, ASTM STP 1232, Philadelphia, 1994, 153.

[7] J.T. Walker, K. Hanson, D. Cadwell, C.W. Keevil, Biofouling 12 (1998) 333.

[8] I.B. Beech, R. Tapper, R. Gubner, in L.V. Evans (Ed.), Biofilms: Recent Advances for Their Study and Control. Harwood, London, (2000) 51.

[9] I.B. Beech, J. Smith, A. Steele, J. Penegar, S. Campbell, Colloids and Surfaces B: Biointerfaces 23 (2002) 231.

[10] F.D.S. Marquis,. in C.A.C. Sequeira, A.K. Tiller (Eds.), Microbial Corrosion-1. Elsevier Applied Science, London (1989) 125.

[11] B. Vuillemin, X. Philippe, R. Oltra, V. Vignal, L. Coudreuse, L.C. Dufour, E. Finot, Corros. Sci. 45 (2003) 1143.

[12] H. Uchida, M. Yamashita, S. Inoue, K. Koterazawa, Mater. Sci. Eng. A 496 (2001) 319.

[13] I. Sekine, M. Yuasa, N. Hirose, T. Tanaki, Prog. Org. Coat. 45 (2002) 1.

[14] M. Khobaib, A. Rensi, T. Matakis, M.S. Donley, Prog. Org. Coat. 41 (2001) 266.

[15] H. Krawiec, V. Vignal, R. Oltra, Electrochem. Commun. 6 (2004) 655.

[16] R. Basséguy, J. Idrac, C. Jacques, A. Bergel, M.L Delia, L. Etcheverry, European Federation of Corrosion Publications n° 45, Local Probe Techniques for Corrosion Research, 5 (2007) 52.

[17] F. L. LaQue, Journal of American Naval Engineering 53 (1941) 29.

[18] N. S. Nikitina and T. B. Ulanovski, Trudy 3 (1957) 190.

[19] A. G. Lagutina, K.P. Danil'Chenko, O.F. Shevenko and V. P. Barrannik, Zashchita Metallov 6 (1970) 48.

[20] A. Mollica and A. Trevis. Proc. 4th Int Congress on marine corrosion and fouling, Antibes, France (1976) 351.

[21] V. Scotto, R. Di Cintio and G. Marcenaro, Corrosion Science 25 (1985) 185.

[22] I. Dupont, D. Féron and G. Novel International biodetioration and biodegradation 41 (1998) 13.

[23] N. Le Bozec, C. Compère, M L'Hers, A.Laouenan, D Costa and P. Marcus. Corrrosion Science 43 (2001) 765.

[24] V. Scotto, M.E. Lai, Corrosion Science 40 (1998) 1007.

[25] beech I B, Microbial today 30 (2003) 115.

[26] S. Da silva, R. Basseguy, A. Bergel, Journal of electroanal. Chem. 561 (2004) 93.

[27] V. L'Hostis, C. Dagbert, D. Feron, Electrochim Acta 48 (2003) 1451.

[28] J.P. Busalmen, M. Vazquez, S. R. de Sanchez, Electrochim. Acta 47 (2002) 1857.

[29] W. Wang, J. Wang, X. Li, H. Xu, J. Wu, Materials corrosion-werkstoffe korrosion 55 (2004) 30.

[30] M.E. Lai and A.Bergel, Journal of Electroanalytical Chemistry 494 (2000) 30.

[31] M.E Lai, V. Scotto, A. Bergel, 10th Int. Congress on Marine Corrosion and Fouling, Melbourne, Australia, (1999) 38.

[32] M.E. Lai and A. Bergel, Bioelectrochemistry 53 (2002) 157.

[33] T.E. Ford, J.S. Maki, R. Mitchell, Corrosion 87, NACE, Houston, TX, USA, (1987) 380.

Caption

Figure 1: Schematic representation of the experimental setup for SVET analysis under polarization.

Figure 2: Cyclic Voltammograms obtained in 0.50M NaCl on graphite electrodes with or without hemin (scan rate: 0.1 V s^{-1}).

Figure 3: Cyclic Voltammograms obtained in 0.50M NaCl on stainless steel electrodes with or without hemin (scan rate: 0.01 V s^{-1}).

Figure 4: Local current map (3D) obtained by SVET in 0.001M NaCl at -0.35 V/SCE on graphite. A: control without hemin. B: Interface hemin / no hemin.

Figure 5: Local current map (3D) obtained by SVET in 0.001M NaCl at -0.50 V/SCE on stainless steel. A: control without hemin. B: Interface hemin / no hemin.

Figure 6: Micrograph of stainless steel surface with hemin deposited in the centre.

Figure 7: Local current map (3D) obtained by SVET at -0.35V/SCE in 0.001M NaCl on graphite. (Hemin deposited in centre)

Figure 8: Local current map (3D) obtained by SVET at -0.5V/SCE in 0.001M NaCl on stainless steel. (Hemin deposited in centre)

Figure 9: Local current map (3D) obtained by SVET at -0.35V/SCE in 0.001M NaCl on graphite: (Hemin deposited around a central clean zone)

Figure 10: Local current map (3D) obtained by SVET in 0.001M NaCl at open circuit potential on graphite. A: control without hemin. B: Interface hemin / no hemin.

Figure 11: Local current map (3D) obtained by SVET in 0.001M NaCl at open circuit potential on stainless steel. A: control without hemin. B: Interface hemin / no hemin.

Figure 1

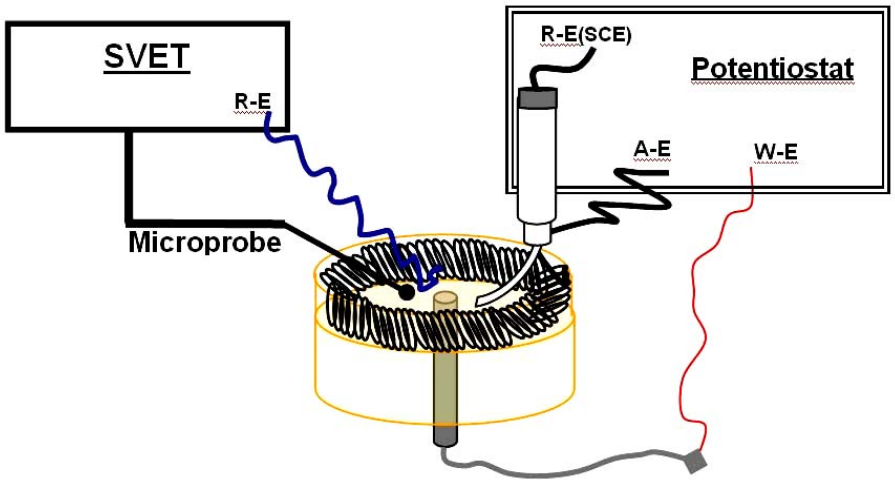

Figure 2

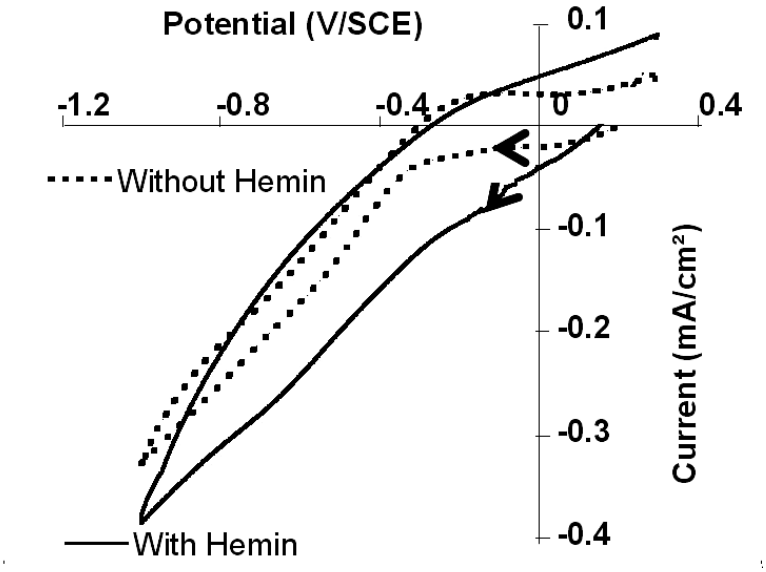
Potential (V/SCE)
0.1
-1.2
-0.8
-0.4
0
0.4
Without Hemin
-0.1
-0.2
-0.3
-0.4
Current (mA/cm²)
With Hemin

Figure 3

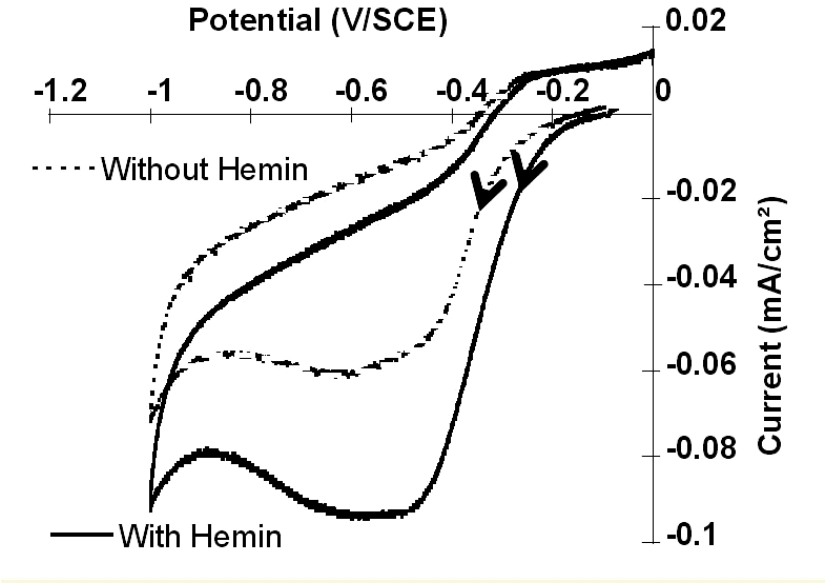
Potential (V/SCE)
0.02
-1.2
-1
-0.8
-0.6
-0.4
-0.2
0
Without Hemin
-0.02
-0.04
-0.06
-0.08
-0.1
Current (mA/cm²)
With Hemin

Figure 4

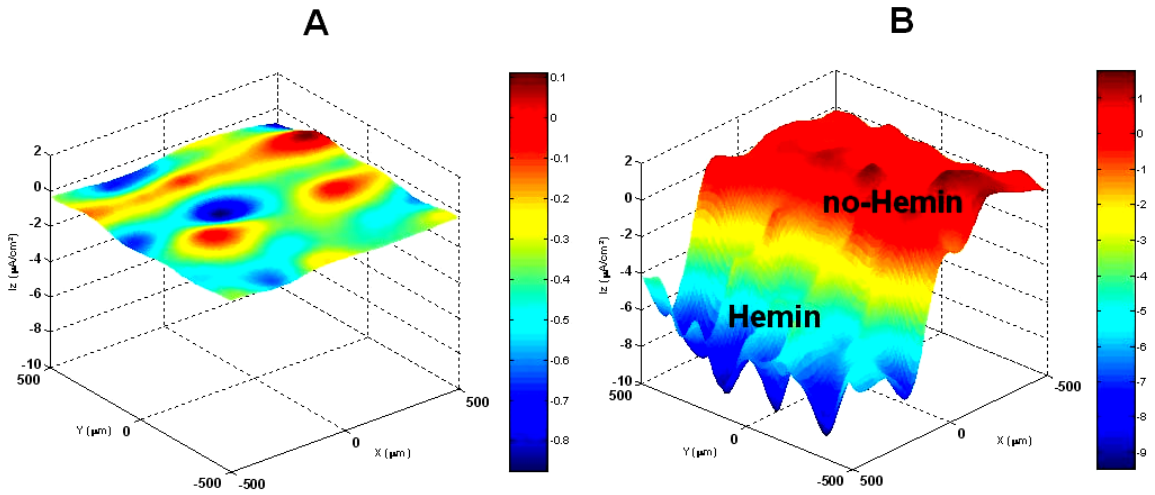

Figure 5

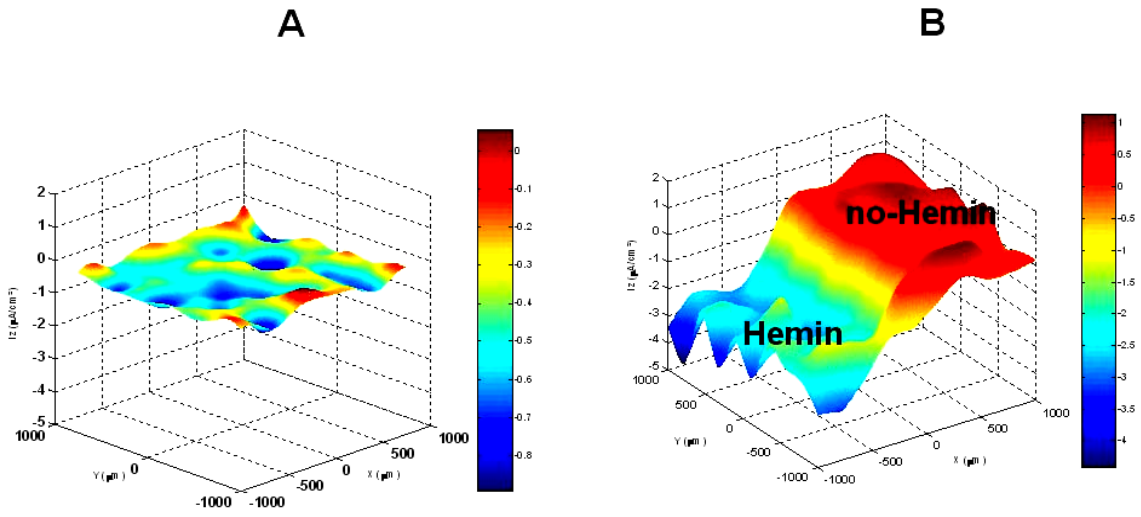

Figure 6

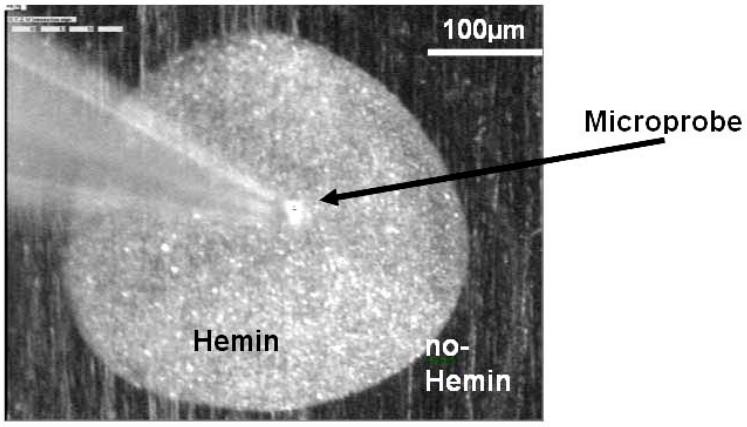

Figure 7

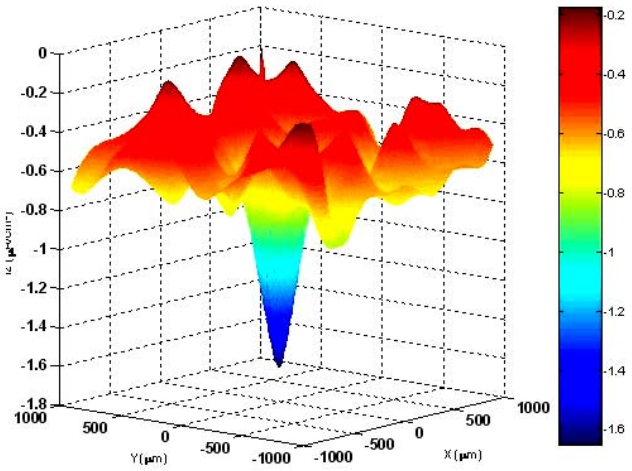
0
-0.2
-0.4
-0.6
-0.8
-1
-1.2
-1.4
-1.6
-1.8
1000
500
0
-500
-1000
Y(μm)
-1000
-500
0
500
1000
X(μm)
-0.2
-0.4
-0.6
-0.8
-1
-1.2
-1.4
-1.6

Figure 8

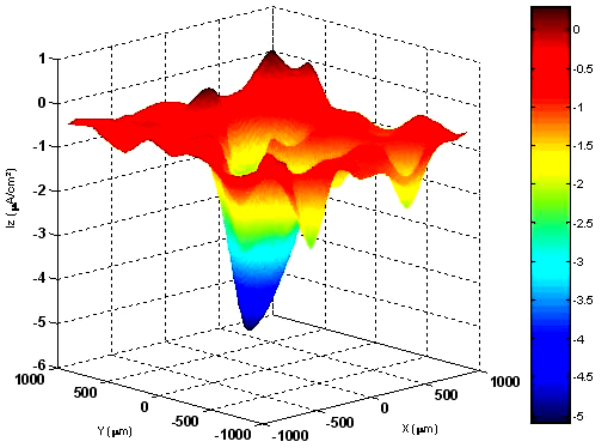
Iz (μA/cm²)
1
0
-1
-2
-3
-4
-5
-6
1000
500
0
-500
-1000
Y (μm)
-1000
-500
0
500
1000
X (μm)
0
-0.5
-1
-1.5
-2
-2.5
-3
-3.5
-4
-4.5
-5

Figure 9

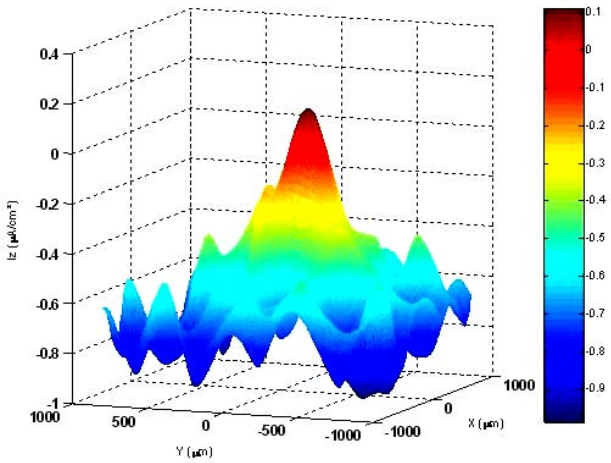
0.4
0.2
0
-0.2
-0.4
-0.6
-0.8
-1
1000
500
0
-500
-1000
Y (µm)
-1000
0
1000
X (µm)
0.1
0
-0.1
-0.2
-0.3
-0.4
-0.5
-0.6
-0.7
-0.8
-0.9

Figure 10

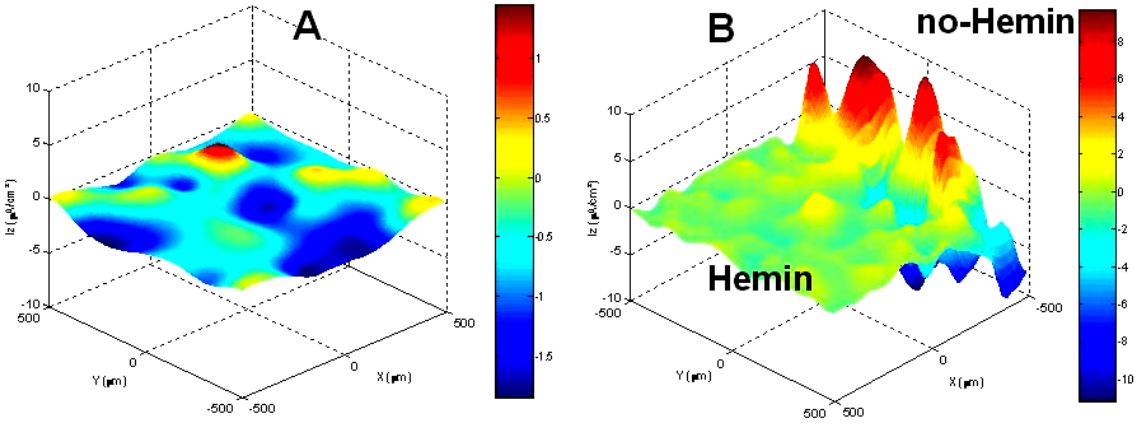

Figure 11